Ru[illegible] M[illegible] [illegible] NiO_3 [illegible]

Oleksandr I. Malyi* and Alex Zunger

TABLE I. Summary of the structural, magnetic, and basic electronic properties observed in different $YNiO_3$ phases. DLE denotes double local environment; SLE denotes single local environment , whereas "B" and "M" refer to bond and magnetic motifs.

Phase	Crystal space group	Magnetic order	Electronic properties	Temperature (K)	Structural motif	Magnetic motif
α	$2_1/$ (Monoclinic)	AFM	Insulator	$<$ 145 [18,32,33]	B-DLE	M-DLE
β	$2_1/$ (Monoclinic)	PM	Insulator	145 $<$ $<$ 582 [18,32,33]	B-DLE	M-DLE
γ	(Orthorhombic)	PM	Metal	$>$582 K [18]	B-SLE	M-SLE

[8,21–23] are mostly regarded as unresponsive background that is not the cause of the formation of (i)–(iii) but effects that can be considered later. This viewpoint caused an understandable migration of computational efforts that aim to describe phases (i)–(iii) of open-shell -electron oxides (e.g., $YNiO_3$ [24–28] and $LaTiO_3$ [10,13]) towards strongly correlated methods, leapfrogging mean-field–like methods such as DFT. However, it remains unclear if DFT was thought to fail in this problem because of its inability to describe strong correlation gap formation in the insulating phases (i) and (ii), or because of the lack of proper description of the local motifs in PM phases (ii) and (iii). For instance, it has been recently demonstrated that accounting for energy-lowering formation of distribution of local spin

FIG. 1. Octahedral volume (first row), local magnetic moments on Ni sublattice (second row), and electronic density of states (third row) from the first-principles calculations of $YNiO_3$. The four columns describe these results as obtained by a sequence of approximations: Column (a) uses a hypothetical monomorphous structure without symmetry breaking (SB), indicating a single characteristic volume and a simple distribution of local moments leading to a metallic zero band gap. Column (b) uses a spin polymorphous structure obtained by replacing an average monomorphous unit cell with a polymorphous supercell structure. This creates a distribution of different octahedral volumes and a

FIG. 2. Schematic illustration of (i-v) different moment (M) and bond (B) environments in $YNiO_3$ and transitions between them used to identify the band-gap opening and metallization. Bold frames denote physical phases from Table I.

SLE" can thus be represented by repeating as a single repeated motif ("monomorphous"). The next step [Fig. 2(ii)] illustrates a unit cell made of a mixed B-SLE with M-DLE, whereas Fig. 2(iii) illustrates the case of a bond-DLE (characterized by two different octahedra, small and large), and moment-DLE (characterized by two different magnetic motifs-zero or finite moment). Different periodic assemblies of bond- and moment-SLE and -DLE motifs make up phases of the crystal realized in crystallographic (monoclinic or orthorhombic) and spin (antiferromagnetic and paramagnetic). For example, the fully disproportionated unit cell of B-DLE/M-DLE can exist in an AFM monoclinic phase [Fig. 2(iii)], or as a PM monoclinic phase [Fig. 2(iv)], or a PM orthorhombic phase [Fig. 2(v), etc.].

We next describe the first-principles results in the seque

af atansiformtion aehosw an oig.

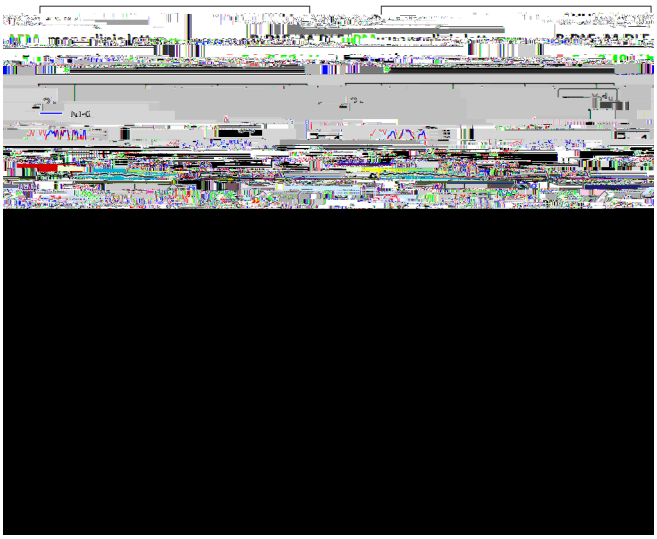

FIG. 5. Néel AFM α to PM

which splits degenerate bands into occupied and empty. We point out that the existence of a gapped PM phase can be naturally described by mean-field DFT without recourse to a strong correlation. This generally requires that one allows for a larger than a minimal unit cell, enabling structural and/or magnetic symmetry breaking. This leads to a polymorphous structure rather than a virtual averaged structure. Interestingly, $YNiO_3$ has two paramagnetic phases: one at low temperatures being a gapped insulator (β) and one at the higher temperature being ungapped metal (γ). This poses an interesting conundrum as to how those behaviors existing in the same system can be understood. The interesting answer pointed out here is that a gapped insulating phase is evident in first-principles mean-field band theory already via minimizing the internal energy alone in an extended supercell. This leads to a polymorphous network having a distribution of both structural and magnetic motifs (whose average is the irrelevant monomorphous approximant). The motif distribution of this athermal polymorphous structure is inherited by the β phase observed in finite-temperature AIMD. As the temperature increases, AIMD shows that the distinct local structural and magnetic motifs lose their polymorphous distribution; when such geometries are used in band theory, a gapless metallic PM γ phase emerges. Thus, the metallic PM phase emerges from the insulating PM phase not necessarily because of loss of electron correlation but because of thermal motion-induced displacements that alter the electronic band structure.

ACKNOWLEDGMENTS

The work on magnetic symmetry breaking and electronic structure calculations was supported by U.S. Department of Energy, Office of Science, Basic Energy Sciences, Materials Sciences and Engineering Division within Grant No. DE-SC0010467 to University of Colorado, Boulder while using resources of the National Energy Research Scientific Computing Center, which is supported by the Office of Science of the U.S. Department of Energy. The authors also acknowledge the use of computational resources located at the National Renewable Energy Laboratory and sponsored by the Department of Energy's Office of Energy Efficiency and Renewable Energy. Work on structural symmetry breaking and molecular dynamics was supported by NSF-DMREF, Grant No. 1921949. The authors acknowledge the use of Extreme Science and Engineering Discovery Environment (XSEDE) supercomputer resources, which are supported by the National Science Foundation, Grant No. ACI-1548562.

APPENDIX: DFT DETAILS

The first-principles calculations are carried out using plane-wave DFT + as implemented in the Vienna Simulation Package (VASP) [38–40] with PBEsol (Perdew-Burke-Ernzerhof (PBE) functional revised for solids) [41]. For all calculations, a rotationally invariant approach introduced by Dudarev [42] with − values of = 2 eV and = 0 applied on Ni- states is utilized. We recall that in DFT + acts primarily to reduce the mean-field self-interaction in DFT, and thus does not have the same role as in Hubbard model (i.e., strong correlation). The cutoff energies for the plane-wave basis are set to 500 eV for final calculations and 550 eV for volume relaxation. Atomic relaxations are performed until the internal forces are smaller than 0.01 eV/Å unless specified. Analysis of structural properties and visualization of computed results are performed using VESTA [43] and PYMATGEN library [44]. The paramagnetic phase of $YNiO_3$ is simulated by using the special quasirandom structure [45] by decorating a 160-atom supercell with spin up and spin down to create a global zero-moment configuration closest to the high-temperature limit of a random spin paramagnet [31]. AIMD simulations are done using the ensemble with an thermostat for 30 ps with the time step of 1 fs. For AIMD simulations, the averaged density of states for snapshots has been calculated from molecular dynamics snapshots as DOS = $\frac{\sum \text{DOS}}{}$, where DOS of different snapshots are aligned using O-1 core states. The volume of each octahedron was calculated as the convex hull volume for each octahedron. For each AIMD simulation, 200 snapshots are extracted from molecular dynamics simulations after an equilibration period of 10 ps. The distribution of magnetic moments and density of states are computed by averaging of corresponding quantities for 40 snapshots of molecular dynamics simulations after equilibration for 10 ps. The DOS for different snapshots is aligned using O-1 core states.

[1] M. Imada, A. Fujimori, and Y. Tokura, Metal-insulator transitions, Rev. Mod. Phys. **70**, 1039 (1998).

[2] N. Mott, (CRC Press, London, 1990).

[3] P. Schofield, A. Bradicich, R. M. Gurrola, Y. Zhang, T. D. Brown, M. Pharr, P. J. Shamberger, and S. Banerjee, Harnessing the metal—insulator transition of VO_2